J. Anat. (2004) **205**, pp417–432

REVIEW

Transmitter receptors and functional anatomy of the cerebral cortex

Karl Zilles,[1,2] Nicola Palomero-Gallagher[1] and Axel Schleicher[2]

[1]*Institute of Medicine, Research Center Jülich, Germany*
[2]*C. & O. Vogt-Institute of Brain Research, University of Düsseldorf, Germany*

Abstract

The currently available architectonic maps of the human cerebral cortex do not match the high degree of cortical segregation as shown by functional imaging. Such functional imaging studies have demonstrated a considerable number of functionally specialized areas not displayed in the architectonic maps. We therefore analysed the regional and laminar distribution of various transmitter receptors in the human cerebral cortex, because these signalling molecules play a crucial role in cortical functions. They may provide a novel and functionally more relevant insight into the regional organization of the cortex, which cannot be achieved by architectonic observations in cell body- or myelin-stained sections. Serial cryostat sections through whole human hemispheres were used for quantitative receptor autoradiography. The regional and laminar densities of numerous receptors of classic transmitter systems were analysed. Alternating sections were stained for comparisons based on cyto- or myeloarchitectonic criteria. Our results demonstrate that the regional distribution of transmitter receptors reflects well-established cyto- and myeloarchitectonically defined borders of cortical areas, but in addition enables the identification of more cortical areas than previously demonstrated. Moreover, the laminar distribution patterns of a given receptor type in different cortical areas as well as those of different receptor types in the same cortical area reveal novel and functionally relevant data concerning the intracortical organization in the human cerebral cortex.

Key words brain mapping; cortical organization; human brain; receptor autoradiography; transmitter receptor.

Introduction

Most of the anatomical interpretations of functional imaging data are based on the cytoarchitectonic map of Brodmann (1909). The interpretation is based on the assumption that macroscopic landmarks (e.g. fundi or openings of sulci, crowns of gyri) are precise indicators of the borders of cytoarchitectonic areas. This assumption was already doubted by the pioneers of architectonic studies (Brodmann, 1909; Vogt & Vogt, 1919). Moreover, recent studies demonstrate in detail that macroscopical landmarks are not reliably associated with cytoarchitectonically defined borders of cortical areas (Zilles et al. 1997; Amunts et al. 1999, 2000; Geyer et al. 1999, 2000; Grefkes et al. 2001).

Even if we do accept this uncertain method of localizing established areal borders, there remain a number of severe problems with most of the classic cyto- and myeloarchitectonic studies, for a variety of reasons. (1) They are based on a highly observer-dependent, statistically untestable procedure for the identification of often subtle differences between neighbouring cortical areas. (2) They do not take intersubject differences in both the macroscopic and the microscopic (architectonic) structure of the cerebral cortex into account. (3) They differ significantly from the detailed parcellation of the macaque cerebral cortex, which was performed using functionally relevant techniques (axonal tracing or electrophysiology, e.g. the posterior parietal cortex; Cavada & Goldman-Rakic, 1989a,b, 1993; Duhamel et al. 1998; Luppino et al. 1999). (4) They do not explain the detailed functional segregation of the human cerebral

Correspondence
Professor Karl Zilles, Institute of Medicine, Research Center Jülich, D-52425 Jülich, Germany. T: +49 (0)2461 61 3015; F: +49 (0)2461 61 2990; E: k.zilles@fz-juelich.de

Accepted for publication *7 October 2004*

cortex as revealed by modern functional imaging techniques (Roland & Zilles, 1998). For instance, functional imaging studies have revealed subdivisions within BA 44 (Friederici & Kotz, 2003), and distinct functional areas have been identified in the human intraparietal sulcus (Bremmer et al. 2001; Grefkes et al. 2002), which cannot be found in any of the previous cyto- or myeloarchitectonic maps.

Recently, observer-independent and statistically testable procedures for architectonic mapping were introduced (Schleicher et al. 1999, 2000; Zilles et al. 2002b), successfully applied to the microanatomical mapping of the human cerebral cortex (Rademacher et al. 1993, 2001; Geyer et al. 1996, 1999; Amunts et al. 1999, 2000; Grefkes et al. 2001; Morosan et al. 2001) and integrated into functional imaging observations (Zilles et al. 1995; Geyer et al. 1996; Larsson et al. 1999; Bodegård et al. 2000; Binkofski et al. 2000; Young et al. 2003). These advances have not only enabled the determination of hitherto undetected borders (e.g. the further subdivision of BA4, Geyer et al. 1996), but also revealed the extent of intersubject variability in the microscopic structure of the human cerebral cortex (Rademacher et al. 1993, 2001; Geyer et al. 1996, 1999; Amunts et al. 1999, 2000; Grefkes et al. 2001; Morosan et al. 2001). This possibility of integrating data from microanatomical and functional imaging studies has created a powerful tool for the mapping of the cerebral cortex (Roland & Zilles, 1994; Mazziotta et al. 2001).

Despite all of these improvements, a brain tissue preparation of higher functional relevance than that provided by simple cell body- or myelin-staining appears to be necessary to gain novel insights into the functional and structural organization of the human cerebral cortex. The mapping of different receptor binding sites seems to be such an approach, and has recently become a powerful tool to reveal the (receptor-) architectonic organization of the cerebral cortex (Zilles et al. 1995, 2002a,b; Geyer et al. 1996, 1997; Zilles & Palomero-Gallagher, 2001; Morosan et al. in press; Zilles, in press).

The aim of the present study was to determine whether: (1) changes in the laminar distribution patterns and/or mean (averaged over all cortical areas) densities of neurotransmitter receptors reflect areal borders that have previously been defined based on cyto- or myeloarchitectonic criteria; (2) different receptor types present different laminar distribution patterns within a given cortical area; (3) the same receptor type presents varying laminar distribution patterns in different cortical areas; (4) a single receptor type reveals all interareal borders in the cerebral cortex; and (5) changes in the laminar distribution patterns and/or mean densities of neurotransmitter receptors enable the definition of borders that have not been described in the classical cyto- or myeloarchitectonic maps.

In order to clarify the first three points, we examined the distribution of glutamatergic, GABAergic, serotoninergic and cholinergic receptors at a particularly conspicuous and widely accepted border of the human cerebral cortex, i.e. the border between the primary (V1, BA 17) and the secondary (V2, BA 18) visual cortex (Brodmann, 1909). This border is the microstructural counterpart of a functionally important landmark, i.e. the vertical meridian of the visual field. Cytoarchitectonically, the V1/V2 border is characterized by abrupt changes in layer IV, which becomes considerably thinner when moving from area V1 to V2 and abruptly loses the subdivision into three sublayers (i.e. layers IVA, IVB and IVC of area V1). The V1/V2 border is also visible in myelin-stained sections due to the unique presence of a heavily myelinated sublayer within V1 but not V2, i.e. the stripe of Gennari (Brodmann, 1909; Fig. 1c). The myelo- and cytoarchitectonic borders are found at precisely the same location (Zilles et al. 2002a), and Gennari's stripe corresponds to the cytoarchitectonic layer IVB.

In order to determine further whether the laminar distribution pattern of a given receptor varies between cortical areas, we not only examined the laminar distribution patterns of glutamatergic receptors in the visual areas V1 and V2, but also in area 4p, which is the posterior part of the primary motor cortex (BA 4, Geyer et al. 1996) and in the entorhinal cortex.

Finally, the distribution patterns of 16 different receptors were analysed in sections obtained from serially sectioned whole human hemispheres and compared with the cell-body and myelin stainings carried out on adjacent sections, in order to determine whether a given receptor reveals all known as well as hitherto unknown interareal borders in the cerebral cortex.

Materials and methods

The results of receptor autoradiography may be influenced by the pre- and post-mortem conditions of the brain tissue (for a detailed discussion see Zilles et al. 2002b). Consequently, brains ($n = 4$) obtained from patients with no record of neurological or psychiatric

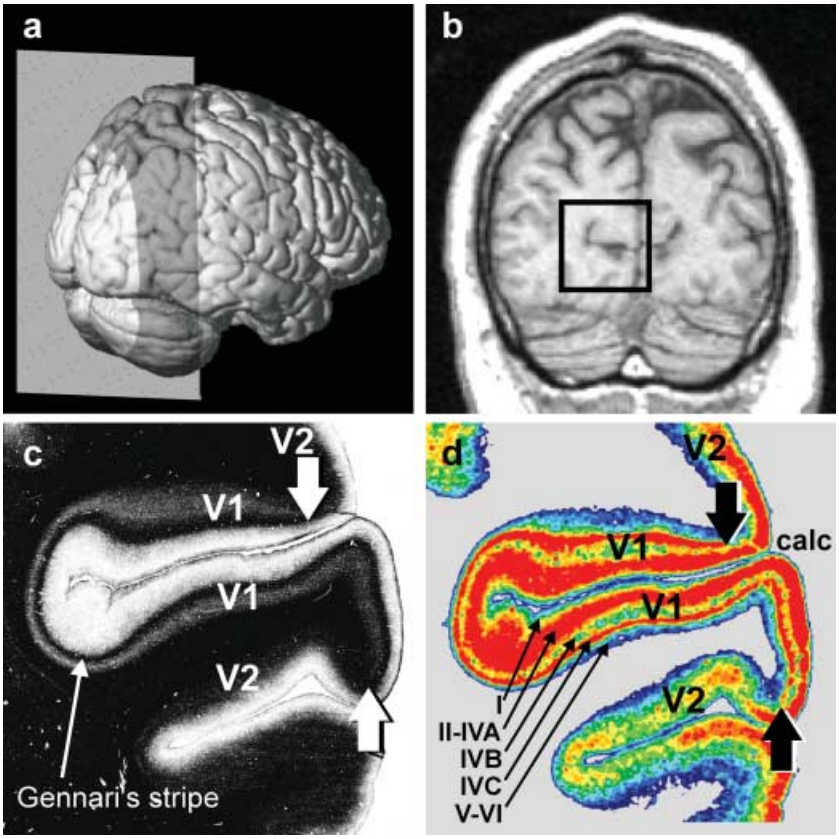

Fig. 1 Lateral view of a three-dimensional reconstruction of a human brain (a). The grey plane marks the position of the MRI section shown in (b). The rectangular frame in (b) highlights the position of the two sections depicted in (c) and (d), which are adjacent to each other. (c) Photomicrograph of a myelin-stained section containing the primary (V1; Brodmann Area (BA) 17) and secondary (V2; BA 18) visual cortices. V1 is characterized by the myelin-dense stripe of Gennari in layer IVC (c), which disappears at the border with V2 (arrowheads), located dorsally and ventrally of V1. (d) Colour-coded autoradiograph in which the regional and laminar distribution of the inhibitory $GABA_A$ receptor was visualized by means of [^{3}H] muscimol. Highest receptor densities (fmol/mg protein) are encoded by red, lowest receptor densities by blue (cf. Figs 5 and 6). The border between V1 and V2 is recognizable by the disappearance of layer IVC of V1, which displays a very high $GABA_A$ receptor density. The areal border between V1 and V2 of the autoradiograph (d) precisely matches the location of this border in the myelin-stained section (c). Note that the small receptor-sparse layer IVB (d) corresponds to Gennari's stripe (c).

diseases (age between 45 and 77 years; three males, one female) were used in the present study. The post-mortem delay was between 8 and 13 h, which is well within the limits described in the literature (e.g. Burke & Greenbaum, 1987; Kontur et al. 1994).

Because chemical or physical fixation of the brain impairs the structure of receptor proteins, and consequently alters the normal binding characteristics of receptors (Zilles & Schleicher, 1995), we used unfixed human brains, which were cut into slabs (2–3 cm thick) at autopsy, frozen and stored at –80 °C. All subjects had given written consent before death and/or had been included in the body donor programme of the Department of Anatomy, University of Düsseldorf, Germany (three brains), or the body donor programme at the UCLA, USA (one brain). Serial cryostat sections (20 μm) were prepared, each comprising the complete cross-sectional area of a hemisphere, using a large-scale cryostat microtome. Adjacent glass-mounted sections were processed for quantitative *in vitro* receptor autoradiography (visualization of glutamatergic AMPA, kainate and NMDA receptors; GABAergic $GABA_A$ and $GABA_B$ receptors; cholinergic nicotinic as well as muscarinic M1 and M2 receptors; serotoninergic 5-HT_{1A} and 5-HT_2 receptors) and for histological staining procedures (Nissl and myelin staining). The determination of specific binding site densities requires the undertaking of two parallel incubation procedures. In one of these, the total binding of a given receptor type is visualized by incubating the sections in a solution containing a specific tritiated receptor ligand. In the other, non-specific binding was determined in adjacent sections by incubation with the tritiated ligand in the presence of an unlabelled compound. Non-specific binding was less than 5% of total binding in all cases. A detailed description of the binding protocols has previously been published (Zilles et al. 2002a,b).

The AMPA receptors were labelled with [^{3}H]AMPA (10 nM) in 50 mM Tris-acetate (pH 7.2) containing 100 mM KSCN for 45 min at 4 °C in the presence of or without quisqualate (10 μM) as unlabelled compound for the determination of non-specific or total binding, respectively. This procedure was followed by four rinses in the buffer (4 s each) at 4 °C. Finally, the sections were dipped twice in 100 mL acetone containing 2.5 mL glutaraldehyde, and dried under a stream of cold air. The

sections were dried under a stream of warm followed by cold air.

The NMDA receptors were labelled with [^{3}H]MK 801 (5 nM) in 50 mM Tris–HCl (pH 7.2) containing 30 μM glycin and 50 μM spermidine for 60 min at 22 °C in the presence of or without (+)MK 801 (100 μM) as unlabelled compound. The incubation was terminated by washing in the buffer (2 × 5 min) and one dip in distilled water at 4 °C. The sections were dried under a stream of cold air.

The kainate receptors were labelled with [^{3}H]kainate (8 nM) in 50 mM Tris–citrate (pH 7.1) containing 10 mM Ca-acetate for 45 min at 4 °C in the presence of or without kainate (100 μM) as unlabelled compound. This procedure was followed by washing in the buffer (3 × 4 s) and two dips in 100 mL acetone containing 2.5 mL glutaraldehyde. The sections were dried under a stream of warm followed by cold air.

The muscarinic M1 receptors were labelled with [^{3}H]pirenzepine (1 nM) in a modified Kreb's buffer (pH 7.4) containing 7 mM K^+ and 37 mM Na^+ for 60 min at 22 °C in the presence of or without unlabelled pirenzepine (10 μM), followed by two washing steps in the buffer for 1 min each and a dip in distilled water at 4 °C. The sections were dried under a stream of cold air.

The muscarinic M2 receptors were labelled with [^{3}H]oxotremorine-M (0.8 nM) in 20 mM HEPES–Tris buffer (pH 7.5) containing 10 mM $MgCl_2$ for 60 min at 22 °C in the presence of or without carbachol (1 μM) as unlabelled compound. This procedure was followed by two washing steps with the buffer for 2 min each and one dip in distilled water at 4 °C. The sections were dried under a stream of cold air.

The nicotinic receptors were labelled with [^{3}H]epibatidine (0.5 nM) in 15 mM HEPES buffer (pH 7.5) containing 120 mM NaCl, 5.4 mM KCl, 0.8 mM $MgCl_2$ and 1.8 mM $CaCl_2$ for 90 min at 22 °C in the presence of or without (–)nicotine-dihydrogentartrate (100 μM). The incubation was terminated by washing in the buffer for 5 min and one dip in distilled water at 4 °C. The sections were dried under a stream of cold air.

The $GABA_A$ receptors were labelled with [^{3}H]muscimol (6 nM) in 50 mM Tris–citrate buffer (pH 7.0) for 40 min at 4 °C in the presence of or without γ-aminobutyric-acid (10 μM) as unlabelled compound followed by three washing steps with the buffer for 3 s each at 4 °C and drying under a stream of cold air.

The $GABA_B$ receptors were labelled with [^{3}H]CGP 54626 (1.5 nM) in 50 mM Tris–HCl buffer (pH 7.2) plus 2.5 mM $CaCl_2$ for 60 min at 4 °C in the presence of or without CGP 55845 (100 μM) as a competitor followed by three washing steps with the buffer for 2 s each and a short dip in distilled water at 4 °C. The sections were dried under a stream of cold air.

The serotonin 5-HT_{1A} receptors were labelled with [^{3}H]8-OH-DPAT (1 nM) in 170 mM Tris–HCl buffer (pH 7.7) plus 4 mM $CaCl_2$ and 0.01% ascorbate for 60 min at 22 °C in the presence of or without 5-hydroxytryptamine (1 μM) as unlabelled compound followed by washing in the buffer for 5 min and three short dips in distilled water at 4 °C. The sections were dried under a stream of cold air.

The serotonin 5-HT_2 receptors were labelled with [^{3}H]ketanserin (0.5 nM) in 170 mM Tris–HCl buffer (pH 7.7) for 120 min at 22 °C in the presence of or without mianserin (10 μM) followed by two washing steps with the buffer for 10 min each and three short dips in distilled water at 4 °C. The sections were then dried under a stream of cold air.

After drying, the sections were exposed to tritium-sensitive films (Hyperfilm, Amersham) for 4–12 weeks depending on the actual ligand. After developing the films, the laminar concentrations of radioactivity were measured by using a previously published procedure (Zilles & Schleicher, 1995; Schleicher et al. 2000; Zilles et al. 2002b). In summary, (1) the autoradiographs were digitized with a digital camera; (2) plastic standards of known radioactivity were used to compute a transformation curve representing the relationship between grey values in the autoradiographs and concentrations of radioactivity in the tissue; (3) these concentration values were transformed into B_{max} values; and (4) the grey values in the autoradiographs were transformed into B_{max} values (e.g. images were linearized). Laminar receptor density profiles, orientated vertically to the cortical surface and layers, and extending from the pial surface (0% cortical depth) to the border between layer VI and white matter (100% cortical depth) were extracted from the linearized images (Schleicher et al. 1999, 2000). Each profile was 210 μm wide. Additionally, linearized autoradiographs were linearly enhanced and contrast colour coded for the sole purpose of visualizing the regional and laminar distribution patterns of the examined receptors.

Results

The neurotransmitter receptors examined show distinct laminar distribution patterns as well as varying

absolute mean (averaged over all cortical layers) densities in the primary (V1) and secondary (V2) visual cortices. These differences allow the border between both areas to be seen clearly.

The laminar distribution patterns in areas V1 and V2 of the $GABA_A$ receptor, the major cortical inhibitory transmitter receptor, are shown in Fig. 1(d). Both areas show drastically different laminar distribution patterns. V1 contains high $GABA_A$ receptor densities in layers II–IVA and IVC, which are interleaved with low densities in layers I, IVB and V–VI. These alternating bands of high and low receptor densities are also reflected in the shape of the density profile depicted in Fig. 2(a). Conversely, V2 shows a more homogeneous distribution of the $GABA_A$ receptors, with highest concentrations in layer III and continuously decreasing densities throughout layers IV–VI. A comparison of the $GABA_A$ autoradiograph with the immediately adjacent, myelin-stained section (Fig. 1c) demonstrates that the $GABA_A$ laminar receptor pattern changes abruptly at the same positions at which the myeloarchitectonic V1/V2 border is located.

The border between V1 and V2 is also revealed by other receptor types, such as the glutamatergic kainate (Fig. 3a) and the cholinergic muscarinic M2 (Fig. 4) receptors, which are visualized in two adjacent coronal sections through a whole human occipital lobe. The dorsal and ventral borders between V1 and V2 are revealed at exactly the same position by both receptor types (see arrows in Figs 3a and 4).

Although all examined receptors revealed the V1/V2 border at exactly the same position, there are pronounced differences in the laminar distribution patterns of each of these receptors within a given area. Thus, one and the same cortical layer of a certain area can contain highest densities of one receptor, but lowest concentrations of another receptor. A more

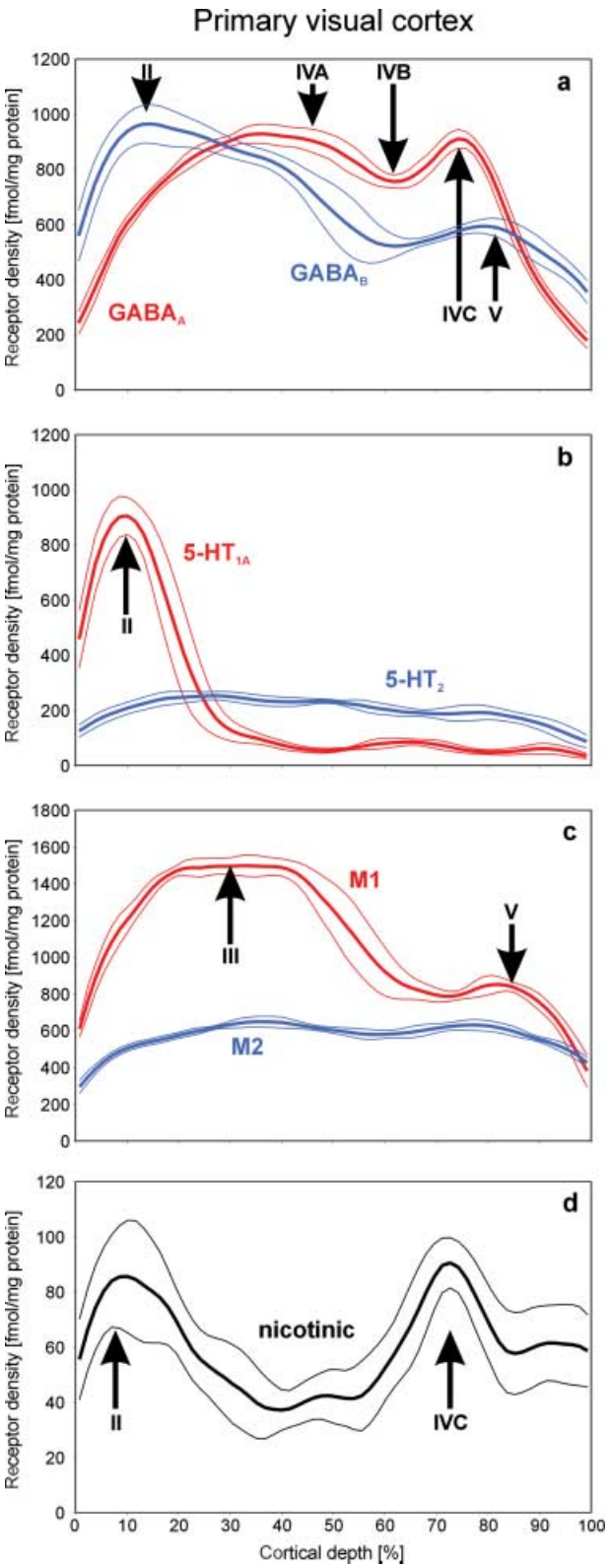

densities), but also show relative maxima and minima in different cortical layers. Therefore, several receptor types within a given region can differ in their mean densities (averaged over all cortical layers) and their laminar distribution patterns.

Fig. 2 Profile curves showing the laminar distribution patterns of the GABAergic $GABA_A$, and $GABA_B$ (a), serotoninergic 5-HT_{1A} and 5-HT_2 (b), cholinergic muscarinic M1 and M2 (c), and cholinergic nicotinic (d) receptors in human V1. The receptor density is expressed in fmol/mg protein, the depth of the cortex is normalized between 0% (pial surface) and 100% (cortex/white matter border). The profile curves represent mean receptor densities averaged over a total of 60 single profiles obtained from three neighbouring sections of a single brain, and dotted lines indicate standard deviations. Roman numerals indicate the position of the respective cortical layers. The receptors examined not only differ considerably in their absolute concentrations (with nicotonic receptors showing the lowest and GABAergic receptors showing the highest

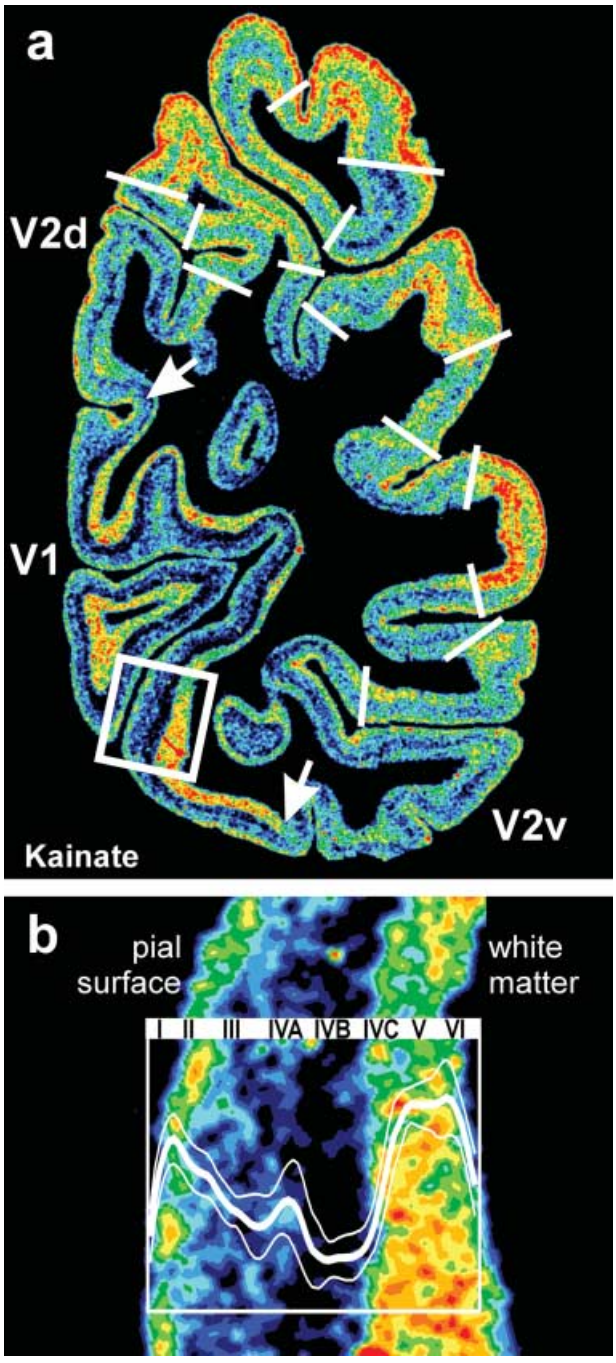

Fig. 3 (a) Regional and laminar distribution patterns of the glutamatergic kainate receptor in a coronal section through the human occipital cortex. The white arrows indicate the dorsal and ventral borders between V1 and V2. For colour coding see legend to Fig. 1. V1 differs from V2 by a lower kainate receptor density in the granular and supragranular layers (layers I–IVC), and by a higher kainate receptor density in the infragranular layers (layers V–VI). Further regional and laminar variations of kainate receptor densities are visible in this section. These local variations of the kainate receptor expression indicate additional borders (white lines) of hitherto unidentified cortical areas (cf. Fig. 4). The position of (b) is indicated by the rectangle in (a). (b) Detailed laminar distribution of the kainate receptor in V1. The profile curve within the inset (bold white line) represents measurements of the kainate receptor densities in V1 from the pial surface to the cortex/white matter border. Dotted lines indicate the standard deviation (cf. Fig. 1). The Roman numerals indicate the position of the cytoarchitectonically defined (by comparison with adjacent cell body-stained sections) cortical layers.

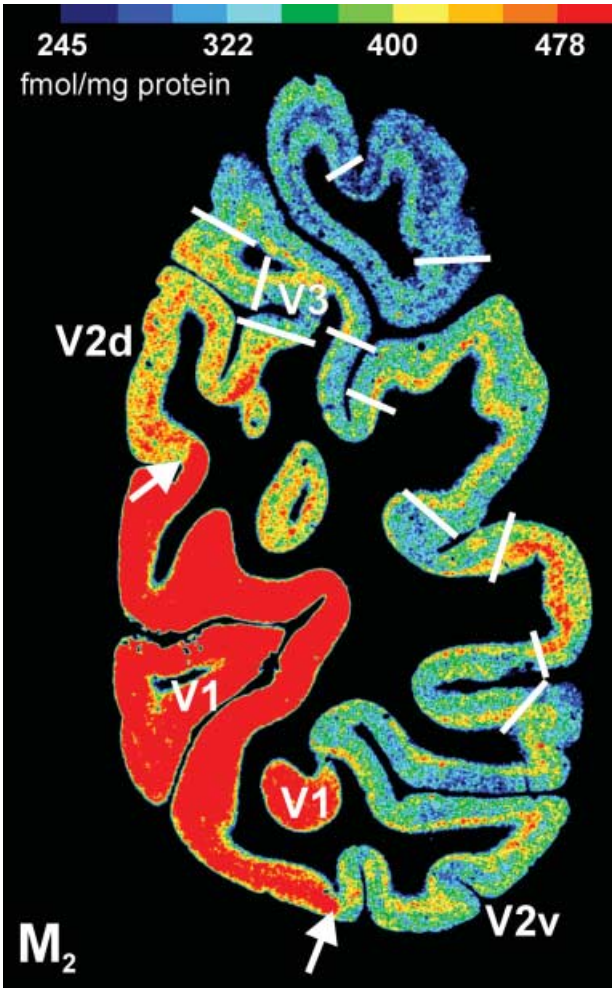

Fig. 4 Coronal section through the occipital part of a human hemisphere showing the distribution pattern of the cholinergic muscarinic M2 receptor. The primary visual cortex V1 is characterized by significantly higher M2 receptor densities than the secondary visual cortex V2. Further local changes of the M2 receptor expression indicate additional borders (white lines) of hitherto unidentified cortical areas. A comparison of these tentative borders with those in the kainate receptor distribution shown in Fig. 3(a) demonstrates again that a single receptor does not show all cortical borders, but when a comparable border is indicated by two or more different receptors, this border is found at precisely the same position.

detailed analysis of the laminar distribution of different receptors in the human primary visual cortex V1 is shown in Figs 2(a–d) and 5(a).

The neurotransmitter GABA mediates inhibitory effects in the cerebral cortex via its major receptor subtypes $GABA_A$ and $GABA_B$. The laminar distribution patterns of these two binding sites in human area V1 are shown in Figs 1(d) and 2(a). Both binding sites exhibit by far the highest absolute densities of all receptors studied in the present observations, but differ slightly in their laminar distribution patterns within V1. Whereas $GABA_A$ shows local maxima in layers II–IVA and IVC, highest $GABA_B$ concentrations are reached in layers I–III and V. Both receptors show an interleaved local minimum in layer IVB (Fig. 2a).

The serotoninergic 5-HT_{1A} receptor reaches an absolute maximum in layer II (Fig. 2b), which is followed by significantly lower densities (approximately ten times lower) in the deeper layers III–VI. Conversely, the serotoninergic 5-HT_2 receptor shows a homogeneous distribution over all cortical layers (Fig. 2b). Therefore, 5-HT_{1A} receptor densities in layer II are approximately five times higher than those of the 5-HT_2 receptors, whereas in layers III–VI the density of the 5-HT_{1A} receptors is half that of the 5-HT_2 receptors.

The cholinergic muscarinic M1 receptor is the clearly prevailing cholinergic subtype in human area V1 (Fig. 2c) when compared with the muscarinic M2 (Fig. 2c) and the nicotinic subtype (Fig. 2d). The M1 receptor reaches an absolute maximum in the supragranular layer III and a second but approximately 50% smaller local maximum in layer V. The M2 subtype is more equally distributed over the cortical layers, whereas the nicotinic receptor displays two distinct maxima in layers II and IVC, respectively. The absolute density of the nicotinic receptor is, however, much lower than that of the muscarinic M1 and M2 subtypes.

Glutamate is the major excitatory neurotransmitter in the human cerebral cortex. Here, we studied its three ionotropic subtypes, i.e. the AMPA, NMDA and kainate receptors (Figs 3b and 5a). The NMDA receptor is the

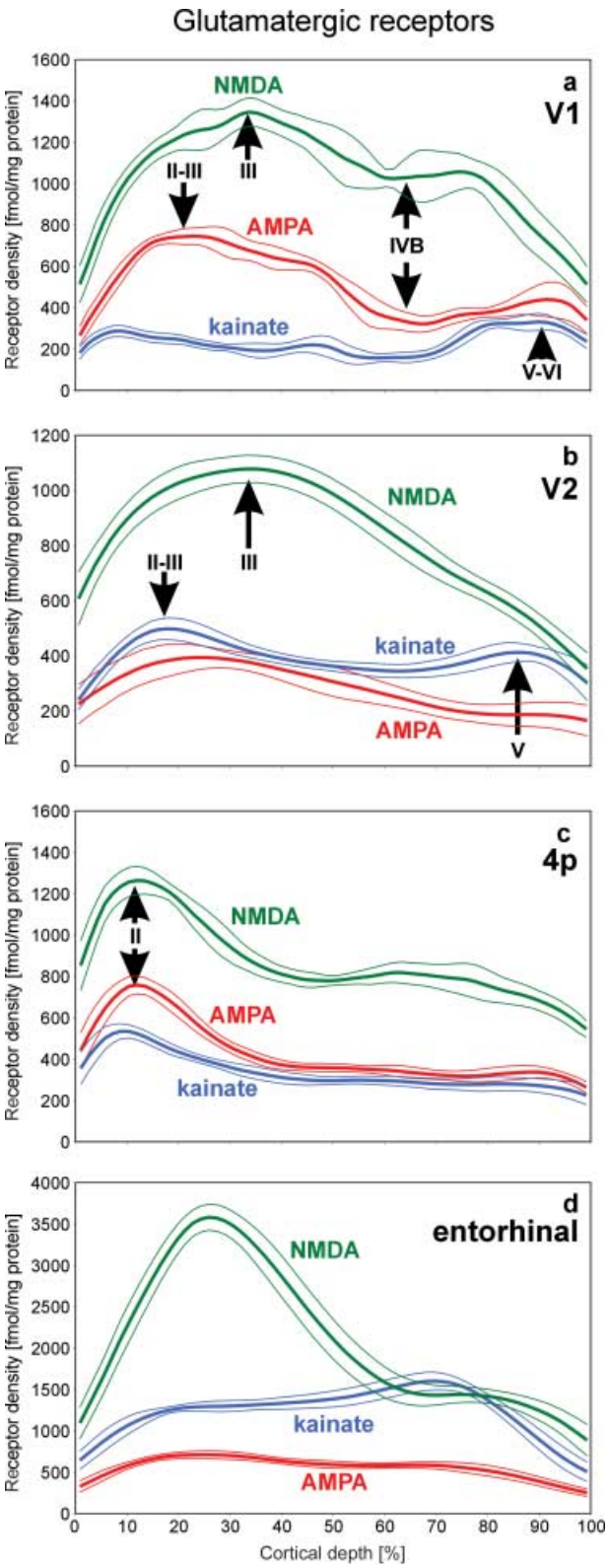

Fig. 5 Laminar distribution patterns of the glutamatergic NMDA, AMPA and kainate receptors in different cortical areas (a, primary visual cortex V1; b, secondary visual cortex V2; c, primary motor cortex 4p, i.e. posterior part of BA 4; d, entorhinal area). The expression of the NMDA receptor reaches highest levels in all four areas relative to the other two glutamatergic receptors, but varies considerably between the areas. The AMPA receptors show higher densities in V1 and 4p, but lower densities in V2 and in the entorhinal cortex when compared with the kainate receptors. Note that the difference in the shape of the kainate receptor density profiles depicted in Fig. 3(b) and in Fig. 5(a) is due solely to differences in the scaling of the *y*-axis.

prevailing subtype in human area V1, followed by the AMPA receptor. The kainate receptor shows the lowest densities. The AMPA and NMDA receptors reach highest densities in layers II–III, with the maximum of the AMPA receptor located slightly more superficially than that of the NMDA receptor. Both receptors show a local minimum in layer IVB. The laminar distribution of the kainate receptor differs significantly from that of the NMDA and AMPA receptors (Fig. 5a). The kainate receptor shows three maxima along its density profile (Fig. 3b). The maximum located in layers IVC–VI contains clearly higher receptor densities than those found in layers I–II and IVA. Kainate receptor densities reach an absolute minimum in layer IVB. Thus, in the overall picture, kainate densities are clearly higher in the infragranular than in the supragranular layers of V1.

The analysis of laminar receptor patterns has shown so far a differential distribution of different receptors in one and the same cortical area, i.e. BA 17, the primary visual cortex. What is the picture when the laminar patterns of the same receptors are compared between different areas? Figure 5(a–d) shows such a comparison of the glutamatergic NMDA, AMPA and kainate receptors between the primary visual cortex V1 (Fig. 5a; see previous paragraph), the secondary visual cortex V2 (Fig. 5b), the primary motor area 4p (Fig. 5c) and, finally, the allocortical entorhinal area (Fig. 5d). The NMDA receptor is the prevailing subtype in all four cortical areas. The AMPA receptor displays the second highest density in V1 and 4p, whereas the kainate receptor reaches the second place in this ranking in V2 and in the entorhinal cortex. Thus, the balance between different receptor subtypes of one transmitter changes between different architectonically and functionally defined areas. The laminar distribution patterns of NMDA and AMPA receptors remain relatively constant and similar if the three neocortical areas V1, V2 and 4p are compared. In all three areas, maxima are found in the supragranular layers and decreasing densities are seen towards the infragranular layers. The kainate receptor reached highest densities in layers IVC–VI of V1, but within V2 and 4p, the highest densities of this subtype are found in layers I–III. The allocortical entorhinal area (Fig. 5d) shows a completely different laminar distribution when compared with the neocortical areas. Although the cytoarchitectonically defined layers of the allocortex are not comparable with those of the neocortex, the profile curves shown in Fig. 5 nevertheless provide an impression of the completely different receptorarchitecture of the entorhinal area when compared with visual and motor areas of the neocortex.

Do different transmitter receptors demonstrate all interareal borders – and at the same position – in the cerebral cortex? Figure 6(a–d) shows neighbouring coronal sections through the central region of a complete human hemisphere in which the muscarinic M2 receptor (Fig. 6a), the nicotinic receptor (Fig. 6b) and the kainate receptor (Fig. 6c) have been visualized. In each of these three different receptor images, local changes of the mean (averaged over all cortical layers) receptor density and its laminar distribution have been identified and labelled by arrows.

It is immediately apparent that the three receptors reveal different aspects of the neurochemical organization of the cerebral cortex, i.e. a single receptor does not reveal all known cortical borders. The M2 receptor displays the relatively highest densities in the primary somatosensory area 3b and the primary auditory area 41, as well as in the mediodorsal thalamic nucleus (MD) and the caudate and putamen. Contrastingly, the kainate receptor reaches the relatively lowest densities in the primary sensory areas 3b and 41 as well as in the motor cortex (areas 4p and 4a), but the highest densities in the polymodal association areas (BA 21 and BA 20) of the temporal lobe. The nicotinic receptor shows a small band of relatively high receptor densities in the primary sensory areas (BA 41 and area 3b) and in the motor cortex, which, at this level of sectioning, consists of the primary motor areas 4a and 4p, the supplementary motor area (SMA) and a part of the cingulate motor cortex.

The most interesting aspect of the differential regional receptor distribution patterns is the fact that numerous borders of the receptorarchitectonically definable areas are found at precisely the same sites irrespective of the receptor type under consideration. This match of border localization based on different receptors corroborates the above described match of the borders of area V1 as determined by $GABA_A$ (Fig. 1c), kainate (Fig. 3a) and M2 (Fig. 4) receptors as well as myelo- and cytoarchitecture. Therefore, although a single receptor type cannot reveal all borders, the 'combination' of borders detected by different receptors does reveal all known borders, as can be seen by a comparison of the receptor-specific borders in Fig. 6(a–c) with the summary sketch of all detectable borders in Fig. 6(d). In this sketch, all borders of cortical areas are labelled, even if

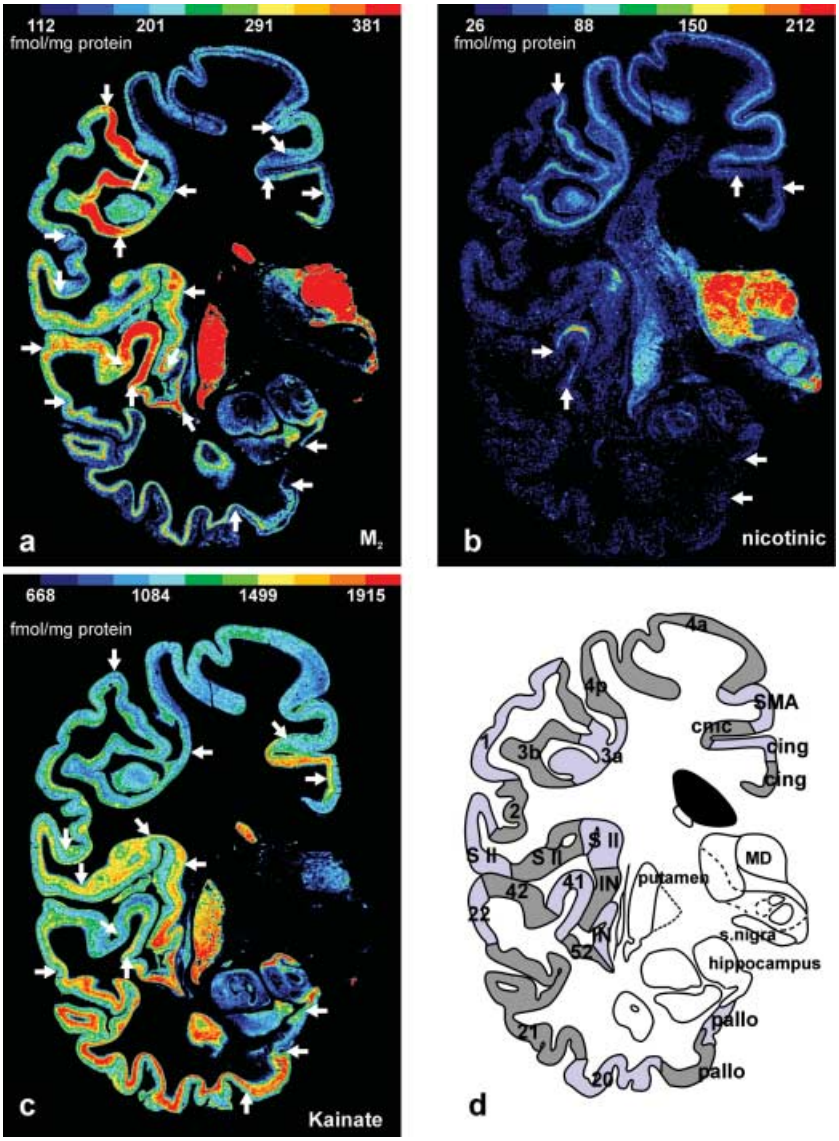

Fig. 6 Adjacent coronal sections through the central part of a human hemisphere in which the cholinergic muscarinic M2 (a), the cholinergic nicotinic (b) and the glutamatergic kainate (c) were visualized by means of [^{3}H]oxotremorine-M, [^{3}H]epibatidine and [^{3}H]kainate, respectively. Local changes in the regional and laminar distribution patterns enable the receptor-based delineation of borders (white arrows in a–c) between cortical areas. None of the single receptor images shows all borders (as displayed in d), but when a given border is revealed by two or more different receptors, this border is found at precisely the same position. If all areal borders detected by autoradiographs of 12 different transmitter receptors are summarized, a complete receptor-based cortical segregation can be presented (as shown in d). This multireceptor map shows all borders demonstrated by the previous cytoarchitectonic observations of Brodmann (1909), but in addition a considerable number of novel areas (e.g. 3a, 3b, 4a, 4p, SMA, cmc, three S II areas, two insular areas) not visible in the classic cytoarchitectonic maps. 1, unimodal somatosensory cortex (BA 1); 2, multimodal parietal cortex (BA 2); 3a, cortical representation of proprioceptive input; 3b, primary somatosensory cortex; 4a and 4p, two subareas of the primary motor cortex; 20, multimodal inferior temporal cortex (BA 20); 21, multimodal middle temporal cortex (BA 21); 22, unimodal acoustic cortex (BA 22); 41, primary auditory cortex (BA 41); 42, secondary auditory cortex (BA 42); 52, parainsular cortex (BA 52); cing, two different areas of the cingulate cortex; cmc, cingulate motor cortex; IN, two different areas of the insular cortex; MD, mediodorsal thalamic nucleus; pallo, two different areas of the periallocortex; S II, three different areas of the secondary somatosensory cortex; SMA, supplementary motor cortex; snigra, substantia nigra.

they are revealed by only one of the three different receptors. For instance, the border between the secondary auditory area 42 and the laterally adjacent area BA 22 is defined by the M2 but not by the nicotinic or kainate receptors (Fig. 6a–c). The most powerful indicator of interareal borders is the M2 receptor, followed by the kainate receptor. The weakest indicator is the nicotinic receptor in these three selected examples.

The last question in this study was whether transmitter receptor distributions only demonstrate interareal borders already established by means of cyto- or myeloarchitectonic studies, or whether they also detect borders that have not been not described in the classical cyto- or myeloarchitectonic maps? Examples for the ability of receptorarchitectonic studies to detect novel cortical areas or subareas hitherto unknown from cyto- or myeloarchitectonic studies can be found in Figs 3, 4 and 6. In Figs 3 and 4, numerous interareal borders (besides those of areas V1, V2d and V2v) are visible in the occipital and superior parietal cortex, which have not been identified in the map of Brodmann (1909) or in other cyto- or myeloarchitectonic studies of the human cerebral cortex. In Fig. 6, three areas can be delineated within the secondary somatosensory cortex (S II), which have not been described until now in the published cytoarchitectonic maps of the human cerebral cortex.

Discussion

The present results demonstrate that changes in the laminar distribution patterns and the mean (averaged over all cortical layers) densities of transmitter receptors not only visualize the cortical borders described in the classical cyto- or myeloarchitectonic maps, but also reveal hitherto unknown interareal borders in the human cerebral cortex. However, none of the examined receptors revealed all known cortical borders. Rather, the distribution patterns of transmitter receptors reveal different aspects of the neurochemical organization of the cerebral cortex, since they enable the determination of 'neurochemical families' of areas.

The laminar distribution patterns of two or more receptor types can differ within a given cortical area. Furthermore, the same receptor type can also present varying laminar distribution patterns in different cortical areas. It is important to stress that the laminar density profiles of receptors do not simply reflect the laminar distribution of the packing density of cell bodies. Such a correlation may have been suggested by the significantly higher mean densities of some receptors in the cell-dense primary sensory areas of the cortex than in the adjacent secondary areas: for instance, the densities of $GABA_A$ or M2 receptors in the primary and secondary visual cortices (V1/V2, Figs 1d and 4), or the densities of the M2 receptors in the primary and secondary auditory cortex (BA 41/BA 42, Fig. 6a). Furthermore, the laminar distribution pattern of the $GABA_A$ receptors, which reached local maxima in the cortical layers with the highest cell density (Figs 1d and 2a), could further support such a supposition. Should such a correlation between receptor density measured by quantitative *in vitro* receptor autoradiography and cell packing density measured by counting cell bodies per volume unit really exist, then receptor density values would only reflect cytoarchitecture. However, regional and laminar receptor densities, as revealed by receptor autoradiography, do not consistently correlate with differences in cell body density in normal brain tissue; for instance, the laminar pattern of the kainate receptor shows, in sharp contrast to that of the $GABA_A$ receptor, intermediate to low densities in the cell-dense supragranular layers, but higher densities in the relatively cell-sparse layer V. The neurobiological basis for this lack of correlation is the fact, that by far the largest number of native receptor complexes, which are demonstrated by their ligand binding sites, are found on dendrites, i.e. in the neuropil, and only to a minor degree on cell bodies. This is in contrast to the visualization of transcripts using *in situ* hybridization for the demonstration of receptor subunits, or to some of the immunohistochemical observations of receptor subunit expression. These latter techniques detect cellular functions occurring completely or preferentially in the cell bodies, and do not necessarily reflect the laminar distribution of the native receptor complex with its binding site (Hall et al. 1997). The independence of the receptor binding sites from the packing densities of neuronal cell bodies is also demonstrated in the present observations. Whereas the densities of $GABA_A$ and nicotinic receptors reach highest values in the most cell-dense layer IVC of the human primary visual cortex V1, the AMPA, NMDA, kainate, $GABA_B$, M1 and $5\text{-}HT_{1A}$ receptors show highest densities in the other, less cell-dense layers of V1 (Figs 3 and 4). Similar results can be obtained by comparisons between the kainate receptor densities (Fig. 5c) of cortical areas of higher (e.g. BAs 41 or 3b) with those of lower cell body densities (e.g. BAs 20 or 21). Thus, the regional and laminar densities of ligand binding sites of native receptor complexes indicate the neurochemical and putative functional segregation of the cerebral cortex independently of cell body or myelin density.

The glutamatergic AMPA receptor is the key molecule for eliciting fast excitatory responses of cortical neurons. The GluR1 subunit of the AMPA receptor has been demonstrated mainly in pyramidal (70%) and

non-pyramidal neurons (29%) of the human prefrontal cortex (He et al. 1996). Most GABAergic interneurons (90%) express the GluR1 subunit. Other subunits of the AMPA receptor are also found preferentially localized in pyramidal neurons of the human prefrontal granular, parietal and temporal association cortex (Vickers et al. 1995). In the present autoradiographic observations, the [^{3}H]AMPA binding sites of the AMPA receptor show a typical bilaminar distribution in the primary visual area V1 with highest densities in layers II/III, intermediate densities in layers V–VI, and low densities in deeper layer III and layer IV. This is in agreement with a previous autoradiographic study (Jansen et al. 1989). In the present study, the AMPA receptors in the secondary visual area V2 and the motor area 4p do not show the bilaminar appearance of V1, but a maximal receptor density in layers II/III followed by a steady decrease down to the lowest densities in layer VI.

Glutamatergic NMDA receptors are found in both pyramidal and non-pyramidal neurons of the human neocortex (Huntley et al. 1997). These receptors play an important role in excitatory synaptic activity and long-term potentiation, although they do not transmit monosynaptic thalamo-cortical input (Salt et al. 1995). NMDA receptors are co-localized with different types of non-NMDA receptors resulting in a large variety of receptor combinations at glutamatergic synapses with different proportions of ionotropic glutamate receptors. mRNAs for NR1, NR2A, NR2B and NR2D receptor subunits were found in pyramidal cells, whereas interneurons express the NR2C subunit (Scherzer et al. 1998), indicating a considerable cell-type-dependent variability of the subunit composition of NMDA receptor complexes.

The [^{3}H]MK-801 binding sites of the NMDA receptor show highest densities in the supragranular layers II–III and intermediate to low densities in granular and infragranular layers of the cortical areas V1, V2, 4p and the entorhinal cortex (Fig. 4). This is in agreement with a previous autoradiographic (Jansen et al. 1989), and immunohistochemical study of the NR1 subunit distribution of the NMDA receptor (Huntley et al. 1997) in the neuropil of the monkey or human neocortex, and an *in situ* hybridization study of the NR1 subunit mRNA in human primary visual area V1 and primary motor cortex 4p (Scherzer et al. 1998). The NR2A subunit mRNA is most densely packed in neuronal cell bodies of layers III, V and VI of the motor cortex, and layers II, III and VI of the visual cortex. The NMDA receptor subunit NR2B mRNA reaches the relatively highest levels in layer II of the primary motor and visual areas. The NR2C subunit mRNA is not detectable in pyramidal neurons, but in glial cells and non-pyramidal neurons. At the lowest absolute level of all NMDA receptor subunits, the NR2C mRNA is most densely accumulated in layers III–VI of the motor and layers II, IVC, V and VI of the visual cortex. Finally, the NRC2D mRNA reaches maximal densities in layers II, V and VI of the motor, and layers IVB and V of the visual cortex. Despite these detailed data regarding the lamina-specific NMDA receptor subunit expression (Scherzer et al. 1998), it is not sufficiently clear from *in situ* hybridization how the native NMDA receptor complexes are composed, particularly with respect to pyramidal or non-pyramidal cell types in the human neocortex.

Glutamatergic kainate receptors of the human cerebral cortex are encoded by the GluR6, GluR7 and KA2 genes (Porter et al. 1997). GluR6 and KA2 mRNAs are found mainly in layers II–III and V–VI (Porter et al. 1997), whereas a GluR 5/6/7 antibody (Vickers et al. 1995) and the GluR7 transcript (Porter et al. 1997) prevail in layers V–VI and are less dense in the superficial layers. In the present observations, the [^{3}H]kainate binding sites show the relatively highest densities in the infragranular layers V–VI of area V1, and in the deeper layers of the entorhinal area. The distribution of kainate receptors in the primary motor area 4p, however, is completely different from that of the other cortical areas as demonstrated in the present paper (Fig. 4). Highest densities are reached in layers I–II of area 4p. Comparable laminar patterns were described by Jansen et al. (1989) both in area V1 and the motor cortex. Thus, both binding and *in situ* hybridization studies show a similar laminar distribution of kainate receptors with some regionally specific variations (e.g. V1 vs. primary motor cortex).

GABA is the major inhibitory transmitter in the human brain. Its binding to the ionotropic $GABA_A$ receptor leads to rapid intracortical inhibition (Alger, 1985). This receptor is present in very high densities in the cerebral cortex (Bowery et al. 1987). GABAergic interneurons are most frequently found in layers II–IVA and IVC of the human primary visual cortex (Blümcke et al. 1990). In previous (Zilles & Schleicher, 1993) and the present observations using [^{3}H]muscimol binding to $GABA_A$ receptors, highest densities of these binding sites are found accordingly in the supragranular layers II–IVA and layer IVC of the human primary visual cortex

(Figs 1d and 3c). The similar laminar distribution of GABA interneurons and $GABA_A$ receptors is in accordance with a localization of these receptors within the limits of terminal fields of GABAergic axons and synapses. A study using a benzodiazepine binding site ligand (Zezula et al. 1988) could not demonstrate high $GABA_A$ receptor densities in human layer IVA. This contrasts not only with previous (Rakic et al. 1988) and present observations of [^{3}H]muscimol binding in human and monkey cortex, which demonstrated high $GABA_A$ receptor densities throughout layers II–IVA, but also with a detailed immunohistochemical study of the $GABA_A$ receptor subunits α1, β2/3 and γ2, which demonstrated high densities of these subunits, particularly of the β2/3 subunits in layer IVA of the human visual cortex (Hendry et al. 1994).

Metabotropic $GABA_B$ receptors occur as postsynaptic receptors and as presynaptic autoreceptors on GABA terminals and also as heteroreceptors on glutamate terminals in the human cerebral cortex (Bonanno et al. 1997). Via presynaptic receptors, GABA inhibits its own release and that of glutamate with similar potencies (for a review see Bonanno & Raiteri, 1993). The [^{3}H]CGP 54626 binding sites of the $GABA_B$ receptors reach highest densities in the cortical layers I–III and much lower densities in the granular and infragranular layers (Fig. 3c), which is similar to earlier findings in the human granular prefrontal cortex (Chu et al. 1987).

Muscarinic receptors were demonstrated immunohistochemically in pyramidal and non-pyramidal neurons of the human neocortex (Schröder et al. 1989a), on which they exert an excitatory effect (for review see Van der Zee & Luiten, 1999). About 30% of the human cortical cholinoceptive neurons express both muscarinic and nicotinic receptors (Schröder et al. 1989a). Using the subtype non-selective (Van der Zee & Luiten, 1999) muscarinic receptor antibody M-35, layers II/III and V show most of the immunoreactive pyramidal cell bodies, whereas layers IV and VI contain a moderate number of round and ovoid immunolabelled cell bodies (Schröder et al. 1989a).

The distribution of M-35 immunoreactive structures is best reflected by the laminar pattern of muscarinic M1 receptors in previous (Rodríguez-Puertas et al. 1997) and the present autoradiographic study. The M1 receptors, which can be located pre- and postsynaptically (Levey, 1996), reach highest densities in layers II–IVA of human V1, with a second, but absolutely lower local maximum in layer V (Fig. 3b). This laminar pattern is in agreement with a previous study of Cortés et al. (1986). M1 receptors are known to be expressed at a more than two-fold higher density than the muscarinic M2 receptor subtype in V1 (Zilles et al. 2002a).

The M1 receptors have a similar laminar distribution pattern in V1 as found for the NMDA receptor (Fig. 4a). Although the spatial resolution of receptor autoradiography does not allow observations at the single cell level, this strikingly similar laminar distribution may suggest a co-localization of both NMDA and M1 receptors. M1 receptors can also influence the dopaminergic neurotransmission and potentiate the GABAergic inhibitory effects of interneurons via pre- and/or postsynaptic mechanisms (Zhong et al. 2003).

Muscarinic M2 receptors are thought to be localized presynaptically as autoreceptors or postsynaptically as heteroreceptors. M2 autoreceptors inhibit cortical acetylcholine release or regulate synaptic transmission as heteroreceptors (Quirion et al. 1994; Douglas et al. 2001; for review see Lucas-Meunier et al. 2003). Previous (Zilles et al. 2002a) as well as the present observations (Figs 5a and 6) demonstrate significantly higher [^{3}H]oxotremorine-M binding site densities in the primary sensory (visual, somatosensory, and auditory) neocortical areas compared with all other neocortical areas. This seems to be an evolutionary conservative aspect of cortical organization, given that a particularly high M2 receptor density was also found in primary sensory areas of non-human primates (Mash et al. 1988). It has been shown that cholinergic function is an important factor of the cortical modulation of sensory input by controlling the signal-to-noise ratio in sensory processing (Sillito & Kemp, 1983; for a recent review see Lucas-Meunier et al. 2003). Cholinergic neurotransmission facilitates the detection and discrimination of tones in the primary auditory cortex, enlarges receptive field size in the somatosensory cortex, and increases orientation and direction selectivity in the primary visual cortex (Sillito & Murphy, 1987; Delacour et al. 1990; Sarter & Bruno, 1997). Although we cannot detect the localization of M2 receptors at the cellular or synaptic level of spatial resolution, the high density of this receptor in the primary sensory areas suggests that the distinct cholinergic effects on thalamo-cortical input may be effected via M2 and nicotinic (see below) receptors.

Nicotinic receptors are present in human cortical pyramidal and non-pyramidal neurons (Schröder et al. 1989b). [^{3}H]Epibatidine, which was used in the present

study, is a high-affinity agonist of central nicotinic acetylcholine receptors (Perry & Kellar, 1995), which labels the $\alpha4\beta2$-like subtype in the human neocortex (Houghtling et al. 1995). Nicotinic receptors show a preferential localization in layers II and IVC of the primary visual cortex V1 (Fig. 3d). Their relatively high density in the primary target region of the geniculocortical input (layer IVC) may be explained by the important role of acetylcholine in the modulation of sensory input (see above). Postsynaptic receptors of the $\alpha7$-like and $\alpha4\beta2$-like subtype are located in the somatodendritic domain of human cortical interneurons (Alkondon et al. 2000). These nicotinic receptor subtypes trigger GABA release, and thus increase the inhibition of pyramidal cells contacted by the interneuron, which leads to an improved signal-to-noise ratio. It has also been demonstrated that presynaptic nicotinic receptors ($\alpha4\beta2$-like nAChRs) are present on the axonal segment or terminal of human cortical GABAergic interneurons synapsing onto a second GABAergic interneuron. These presynaptic nicotinic receptors trigger the GABA release from the first interneuron, and thus increase the inhibition of the second interneuron. This can lead to a disinhibition of postsynaptic pyramidal neurons, and thereby strengthen the thalamo-cortical input (Alkondon et al. 2000). These results emphasize that, depending on its position within intracortical and interregional connectivity, a given receptor type can cause modulations of neurotransmission in opposite directions.

[^{3}H]8-OH-DPAT is a selective 5-HT$_{1A}$ receptor agonist. In the neocortex, this receptor is localized postsynaptically (Radja et al. 1993). The [^{3}H]8-OH-DPAT binding to 5-HT$_{1A}$ receptors shows a clear preference for layers I–II in previous reports (Pazos et al. 1987a; Hall et al. 1997) as well as in the present study. This is not in agreement with the results of *in situ* hybridization studies in the human neocortex, where 5-HT$_{1A}$ receptor mRNA was found in layers II–VI (Pasqualetti et al. 1996) and pyramidal cell bodies particularly in layer III (Burnet et al. 1995) were heavily labelled. This lack of correspondence between receptor autoradiography and *in situ* hybridization data can be explained by a preferential localization of the native receptor complex with its binding site on the peripheral parts of dendrites, because the neurons of the deeper cortical layers show an intensive dendritic arborization in the most superficial cortical layers (Pasqualetti et al. 1996).

5-HT$_2$ receptors are located postsynaptically within the cerebral cortex (Fischette et al. 1987), preferentially on the large apical dendrites of pyramidal cells, and at lower densities on GABAergic interneurons of rhesus monkeys (Jakab & Goldman-Rakic, 1998, 2000). Presynaptic localization of these receptors has also been described using immunocytochemistry (Jakab & Goldman-Rakic, 1998). The 5-HT$_2$ receptors facilitate excitatory firing of pyramidal neurons.

The *in situ* hybridization studies of Burnet et al. (1995) and Pasqualetti et al. (1996) demonstrated the presence of 5-HT$_2$ receptors in layers III–V of the human cerebral cortex. The binding sites of the 5-HT$_2$ receptor antagonist [^{3}H]ketanserin were found to be relatively equally distributed throughout the human cortical layers with some preference of layers III and V (Pazos et al. 1987b). This is in agreement with immunocytochemical observations in rhesus monkeys (Jakab & Goldman-Rakic, 1998). In the present observations, slightly higher 5-HT$_2$ receptor densities were registered in layers III–IVC compared with layers V–VI of the human primary visual cortex V1. This is in agreement with a previous study in this cortical area of monkeys (Rakic et al. 1988; Lidow et al. 1989).

There is a clear spatial dichotomy of the serotonin innervation of the primary visual cortex. The 5-HT$_{1A}$ receptor shows a clear preference for layers I–II, and therefore focuses a major part of the serotoninergic innervation onto these cortical layers. Conversely, the 5-HT$_2$ receptor is not only more homogeneously distributed over all cortical layers, but reaches approximately a 100% higher density in layers III–VI than the 5-HT$_{1A}$ receptor. As a result, there is a major 5-HT$_{1A}$-mediated influence in layers I–II, and a dominating 5-HT$_2$-mediated influence in layers III–VI.

In conclusion, our present observations demonstrate that the regional distribution patterns of transmitter receptors not only reflect well-established cyto- and myeloarchitectonic borders between cortical areas, but also indicate additional borders not visible in cyto- or myeloarchitecture. Thus receptorarchitectonic studies provide a powerful tool to study the microstructural and neurochemical organization of the cerebral cortex and will lead to a more detailed map of the human cerebral cortex, which can be compared with functional imaging data. Because a single receptor does not reveal all borders, only a multireceptor approach is adequate in order to analyse the complex regional segregation of the cortex. Finally, the analysis of the laminar distribution patterns of several receptor types in different cortical areas may provide a link to receptor

and functional data provided by observations at the single cell level, and thus can contribute to a better understanding of the neurochemical organization of intracortical circuitry.

Acknowledgements

This article is based on a talk given at a Symposium of the Anatomical Society of Great Britain and Ireland in January 2004, entitled 'Functional anatomy of the human brain', organized by John Marshall. The work was supported by grants (K.Z.) from the DFG (KFO 112/TP7), the Volkswagen-Stiftung, and the Human Brain Project/Neuroinformatics research funded by the National Institute of Biomedical Imaging and Bioengineering, the National Institute of Neurological Disorders and Stroke, and the National Institute of Mental Health. Our special thanks to Dr A. Toga (UCLA) for one of the deep-frozen hemispheres studied in the present observations.

References

Alger BE (1985) GABA and glycine: postsynaptic actions. In *Neurotransmitter Actions in the Vertebrate Nervous System* (eds Rogawski MA, Barker JL), pp. 33–69. New York: Plenum Press.

Alkondon B, Pereira EFR, Eisenberg HM, Albuquerque EX (2000) Nicotinic receptor activation in human cerebral cortical interneurons: a mechanism for inhibition and disinhibition of neuronal networks. *J. Neurosci*. **20**, 66–75.

Amunts K, Schleicher A, Bürgel U, Mohlberg H, Uylings HBM, Zilles K (1999) Broca's region revisited: Cytoarchitecture and intersubject variability. *J. Comp. Neurol*. **412**, 319–341.

Amunts K, Malikovic A, Mohlberg H, Schormann T, Zilles K (2000) Brodmann's areas 17 and 18 brought into stereotaxic space – where and how variable? *Neuroimage* **11**, 66–84.

Binkofski F, Amunts K, Stephan KM, et al. (2000) Broca's region subserves imagery of motion: a combined cytoarchitectonic and fMRI study. *Human Brain Mapping* **11**, 273–285.

Blümcke I, Hof PR, Morrison JH, Celio MR (1990) Distribution of parvalbumin immunoreactivity in the visual cortex of old world monkeys and humans. *J. Comp. Neurol*. **301**, 417–432.

Bodegård A, Geyer S, Amunts K, Naito E, Zilles K, Roland PE (2000) Somatosensory areas in man activated by moving stimuli. Cytoarchitectonic mapping and PET. *Neuroreport* **11**, 187–191.

Bonanno G, Raiteri M (1993) Multiple $GABA_B$ receptors. *TIPS* **14**, 259–261.

Bonanno G, Fassio A, Schmid G, Severi P, Sala R, Raiteri M (1997) Pharmacologically distinct $GABA_B$ receptors that mediate inhibition of GABA and glutamate release in human neocortex. *Br. J. Pharmacol*. **120**, 60–64.

Bowery NG, Hudson AL, Price GW (1987) $GABA_A$ and $GABA_B$ receptor site distribution in the rat central nervous system. *Neuroscience* **20**, 362–383.

Bremmer F, Schlack A, Shah NJ, et al. (2001) Polymodal motion processing in posterior parietal and premotor cortex. a human fMRI study strongly implies equivalencies between humans and monkeys. *Neuron* **29**, 287–296.

Brodmann K (1909) *Vergleichende Lokalisationslehre der Großhirnrinde in ihren Prinzipien dargestellt auf Grund des Zellenbaues*. Leipzig: Barth. English translation, Garey LJ (1994) *Brodmann's 'Localisation in the Cerebral Cortex'*. London: Smith-Gordon.

Burke RE, Greenbaum D (1987) Effect of postmortem factors on muscarinic receptor subtypes in rat brain. *J. Neurochem*. **49**, 592–596.

Burnet PWJ, Eastwood SL, Lacey K, Harrison PJ (1995) The distribution of 5-HT_{1A} and 5-HT_{2A} receptor mRNA in human brain. *Brain Res*. **676**, 157–168.

Cavada C, Goldman-Rakic PS (1989a) Posterior parietal cortex in rhesus monkey. I. Parcellation of areas based on distinctive limbic and sensory corticocortical connections. *J. Comp. Neurol*. **287**, 393–421.

Cavada C, Goldman-Rakic PS (1989b) Posterior parietal cortex in rhesus monkey. II. Evidence for segregated corticocortical networks linking sensory and limbic areas with the frontal lobe. *J. Comp. Neurol*. **287**, 422–445.

Cavada C, Goldman-Rakic PS (1993) Multiple visual areas in the posterior parietal cortex of primates. In *Progress in Brain Research* (eds Hicks TP, Molotchnikoff S, Ono T), Vol. 95, pp. 123–137. Amsterdam: Elsevier.

Chu DCM, Penney JB, Young AB (1987) Cortical $GABA_B$ and $GABA_A$ receptors in Alzheimer's disease: a quantitative autoradiographic study. *Neurology* **37**, 1454–1459.

Cortés R, Probst A, Tobler H-J, Palacios JM (1986) Muscarinic cholinergic receptor subtypes in the human brain. II. Quantitative autoradiographic studies. *Brain Res*. **362**, 239–253.

Delacour J, Houcine O, Costa JC (1990) Evidence for a cholinergic mechanisms of 'learned' changes in the responses of barrel field neurons of the awake and undrugged rat. *Neuroscience* **34**, 1–8.

Douglas CL, Baghdoyan HA, Lydic R (2001) M2 muscarinic autoreceptors modulate acetylcholine release in prefrontal cortex of C57BL/6J mouse. *J. Pharmacol. Exp. Ter*. **299**, 960–966.

Duhamel JR, Colby CL, Goldberg ME (1998) Ventral intraparietal area of the macaque: Congruent visual and somatic response properties. *J. Neurophysiol*. **79**, 126–136.

Fischette CT, Nock B, Renner K (1987) Effects of 5,7-dihydroxytryptamine on serotonin1 and serotonin2 receptors throughout the rat central nervous system using quantitative autoradiography. *Brain Res*. **421**, 263–279.

Friederici AD, Kotz SA (2003) The brain basis of syntactic processes: functional imaging and lesion studies. *Neuroimage* **20**, S8–S17.

Geyer S, Ledberg A, Schleicher A, et al. (1996) Two different areas within the primary motor cortex of man. *Nature* **382**, 805–807.

Geyer S, Schleicher A, Zilles K (1997) The somatosensory cortex of human: Cytoarchitecture and regional distributions of receptor-binding sites. *Neuroimage* **6**, 27–45.

Geyer S, Schleicher A, Zilles K (1999) Areas 3a, 3b, and 1 of human primary somatosensory cortex: 1. Microstructural organization and interindividual variability. *Neuroimage* **10**, 63–83.

Geyer S, Schormann T, Mohlberg H, Zilles K (2000) Areas 3a, 3b, and 1 of human primary somatosensory cortex. 2. Spatial normalization to standard anatomical space. *Neuroimage* **11**, 684–696.

Grefkes C, Geyer S, Schormann T, Roland P, Zilles K (2001) Human somatosensory area 2: observer-independent cytoarchitectonic mapping, interindividual variability, and population map. *Neuroimage* **14**, 617–631.

Grefkes C, Weiss PH, Zilles K, Fink GR (2002) Crossmodal processing of object features in human anterior intraparietal cortex: an fMRI study strongly implies equivalencies between humans and monkey. *Neuron* **35**, 173–184.

Hall H, Lundkvist C, Halldin C, et al. (1997) Autoradiographic localization of 5-HT_{1A} receptors in the post-mortem human brain using [^{3}H]WAY-100635 and [^{11}C]WAY-100635. *Brain Res*. **745**, 96–108.

He Y, Ong WY, Leong SK, Garey LJ (1996) Distribution of glutamate receptor subunit GluR1 and GABA in human cerebral neocortex. A double immunolabelling and electron microscopic study. *Exp*. *Brain Res*. **112**, 147–157.

Hendry SHC, Huntsman M-M, Viòuela A, Möhler H, de Blas AL, Jones EG (1994) $GABA_A$ receptor subunit immunoreactivity in primate visual cortex. Distribution in macaques and humans and regulation by visual input in adulthood. *J*. *Neurosci*. **14**, 2383–2401.

Houghtling RA, Dávila-García MI, Kellar KJ (1995) Characterization of (±)-[^{3}H]epibatidine binding to nicotinic cholinergic receptors in rat and human brain. *Mol*. *Pharmacol*. **48**, 280–287.

Huntley GW, Vickers JC, Morrison JH (1997) Quantitative localization of NMDAR1 receptor subunit immunoreactivity in inferotemporal and prefrontal association cortices of monkey and man. *Brain Res*. **749**, 245–262.

Jakab RL, Goldman-Rakic PS (1998) 5-Hydroxytryptamine$_{2A}$ serotonin receptors in the primate cerebral cortex: possible site of action of hallucinogenic and antipsychotic drugs in pyramidal cell apical dendrites. *Proc*. *Natl Acad*. *Sci*. *USA* **95**, 735–740.

Jakab RL, Goldman-Rakic PS (2000) Segregation of serotonin 5-HT_{2A} and 5-HT_3 receptors receptors in inhibitory circuits of the primate cerebral cortex. *J*. *Comp*. *Neurol*. **417**, 337–348.

Jansen KLR, Faull RLM, Dragunow M (1989) Excitatory amino acid receptors in the human cerebral cortex: a quantitative autoradiographic study comparing the distributions of [^{3}H]TCP, [^{3}H]glycine, L-[^{3}H]glutamate, [^{3}H]AMPA and [^{3}H]kainic acid binding sites. *Neuroscience* **32**, 587–607.

Kontur PJ, al-Tikriti M, Innis RB, Roth RH (1994) Postmortem stability of monoamines, their metabolites and receptor binding in rat brain regions. *J*. *Neurochem*. **62**, 282–290.

Larsson J, Amunts K, Gulyás B, Malikovic A, Zilles K, Roland PE (1999) Neuronal correlates of real and illusory contour perception: functional anatomy with PET. *Eur*. *J*. *Neurosci*. **11**, 4024–4036.

Levey AI (1996) Muscarinic acetylcholine receptor expression in memory circuits: Implications for treatment of Alzheimer's disease. *Proc*. *Natl Acad*. *Sci*. *USA* **93**, 13541–13546.

Lidow MS, Goldman-Rakic PS, Gallager DW, Rakic P (1989) Quantitative autoradiographic mapping of serotonin 5-HT_1 and 5-HT_2 receptors and uptake sites in the neocortex of the rhesus monkey. *J*. *Comp*. *Neurol*. **280**, 27–42.

Lucas-Meunier E, Fossier P, Baux G, Amar M (2003) Cholinergic modulation of the cortical neuronal network. *Pflügers Arch*. – *Eur*. *J*. *Neurophysiol*. **446**, 17–29.

Luppino G, Murata A, Govoni P, Matelli M (1999) Largely segregated parietofrontal connections linking rostral intraparietal cortex (areas AIP and VIP) and the ventral premotor cortex (areas F5 and F4). *Exp*. *Brain Res*. **128**, 181–187.

Mash DC, White WF, Mesulam M-M (1988) Distribution of muscarinic receptor subtypes within architectonic subregions of the primate cerebral cortex. *J*. *Comp*. *Neurol*. **278**, 265–274.

Mazziotta J, Toga A, Evans A, et al. (2001) A probabilistic atlas and reference system for the human brain: International Consortium for Brain Mapping (ICBM). *Phil*. *Trans*. *R*. *Soc*. *London, Biol*. *Sci*. **356**, 1293–1322.

Morosan P, Rademacher J, Schleicher A, Amunts K, Schormann T, Zilles K (2001) Human primary auditory cortex: Cytoarchitectonic subdivisions and mapping into a spatial reference system. *Neuroimage* **13**, 684–701.

Morosan P, Rademacher J, Palomero-Gallagher N, Zilles K (2004) Anatomical organization of the human auditory cortex: Cytoarchitecture and transmitter receptors. In *Auditory Cortex – Towards a Synthesis of Human and Animal Research* (eds Heil P, König E, Budinger E), pp. 27–50. Mahwah, NJ: Lawrence Erlbaum.

Pasqualetti M, Nardi I, Ladinsky H, Marazitti D, Cassano GB (1996) Comparative anatomical distribution of serotonin 1, 1Dα and 2A receptor mRNAs in human brain postmortem. *Mol*. *Brain Res*. **39**, 223–233.

Pazos A, Probst A, Palacios JM (1987a) Serotonin receptors in the human brain. III. Autoradiographic mapping of serotonin-1 receptors. *Neuroscience* **21**, 97–122.

Pazos A, Probst A, Palacios JM (1987b) Serotonin receptors in the human brain. IV. Autoradiographic mapping of serotonin-2 receptors. *Neuroscience* **21**, 123–139.

Perry DC, Kellar KJ (1995) [^{3}H]Epibatidine labels nicotinic receptors in rat brain: An autoradiographic study. *J*. *Pharmacol*. *Exp*. *Ther*. **275**, 1030–1034.

Porter RHP, Eastwood SL, Harrison PJ (1997) Distribution of kainate receptor subunit mRNAs in human hippocampus, neocortex and cerebellum, and bilateral reduction of hippocampal GluR6 and KA2 transcripts in schizophrenia. *Brain Res*. **751**, 217–231.

Quirion R, Richard J, Wilson A (1994) Muscarinic and nicotinic modulation of cortical acetylcholine release monitored by in vivo microdialysis in freely moving adult rats. *Synapse* **17**, 92–100.

Rademacher J, Caviness J, Steinmetz H, Galaburda AM (1993) Topographical variation of the human primary cortices: implications for neuroimaging, brain mapping, and neurobiology. *Cereb*. *Cortex* **3**, 313–329.

Rademacher J, Morosan P, Schormann T, et al. (2001) Probabilistic mapping and volume measurement of human primary auditory cortex. *Neuroimage* **13**, 669–683.

Radja F, Descarries L, Dewar KM, Reader TA (1993) Serotonin 5-HT_1 and 5-HT_2 receptors in adult brain after neonatal

destruction of nigrostriatal dopamine neurons: a quantitative autoradiographic study. *Brain Res*. **606**, 273–285.

Rakic P, Goldman-Rakic PS, Gallager D (1988) Quantitative autoradiography of major neurotransmitter receptors in the monkey striate and extrastriate cortex. *J. Neurosci*. **8**, 3670–3690.

Rodríguez-Puertas R, Pascual J, Vilaró T, Pazos A (1997) Autoradiographic distribution of M1, M2, M3, and M4 muscarinic receptor subtypes in Alzheimer's disease. *Synapse* **26**, 341–350.

Roland PE, Zilles K (1994) Brain atlases – A new research tool. *TINS* **17**, 458–467.

Roland PE, Zilles K (1998) Structural divisions and functional fields in the human cerebral cortex. *Brain Res. Rev*. **26**, 87–105.

Salt TE, Meir CL, Seno N, Krucker T, Herrling PL (1995) Thalamocortical and corticocortical excitatory postsynaptic potentials mediated by excitatory amino acid receptors in the cat motor cortex in vivo. *Neuroscience* **64**, 433–442.

Sarter M, Bruno JP (1997) Cognitive functions of cortical acetylcholine: toward a unifying hypothesis. *Brain Res. Rev*. **23**, 28–46.

Scherzer CR, Landwehrmeyer GB, Kerner JA, et al. (1998) Expression of N-methyl-D-aspartate receptor subunit mRNAs in the human brain: Hippocampus and cortex. *J. Comp. Neurol*. **390**, 75–90.

Schleicher A, Amunts K, Geyer S, Morosan P, Zilles K (1999) Observer-independent method for microstructural parcellation of cerebral cortex: a quantitative approach to cytoarchitectonics. *Neuroimage* **9**, 165–177.

Schleicher A, Amunts K, Geyer S, et al. (2000) A stereological approach to human cortical architecture: identification and delineation of cortical areas. *J. Chem. Neuroanat*. **20**, 31–47.

Schröder H, Zilles K, Maelicke A, Hajos F (1989a) Human cortical neurons contain both nicotinic and muscarinic acetylcholine receptors: an immunocytochemical double-labeling study. *Synapse* **4**, 319–326.

Schröder H, Zilles K, Maelicke A, Hajos F (1989b) Immunohisto- and cytochemical localization of cortical nicotinic cholinoceptors in rat and man. *Brain Res*. **502**, 287–295.

Sillito AM, Kemp JA (1983) Cholinergic modulation of the functional organization of the cat visual cortex. *Brain Res*. **289**, 143–155.

Sillito AM, Murphy PC (1987) The cholinergic modulation of cortical function. *Cerebral Cortex* **6**, 161–185.

Van der Zee EA, Luiten PGM (1999) Muscarinic acetylcholine receptors in the hippocampus, neocortex and amygdala. A review of immunocytochemical localization in relation to learning and memory. *Prog. Neurobiol*. **58**, 409–471.

Vickers JC, Huntley GW, Hof PR, Bederson J, DeFelipe J, Morrison JH (1995) Immunocytochemical localization of non-NMDA ionotropic excitatory amino acid receptor subunits in human neocortex. *Brain Res*. **671**, 175–180.

Vogt C, Vogt O (1919) Allgemeinere Ergebnisse unserer Hirnforschung. *J. Psychol. Neurol*. **25**, 292–398.

Young JP, Geyer S, Grefkes C, et al. (2003) Regional cerebral blood flow correlations of somatosensory areas 3a, 3b, 1, and 2 in humans during rest. A PET and cytoarchitectural study. *Human Brain Mapping* **19**, 183–196.

Zezula J, Cortés R, Probst A, Palacios JM (1988) Benzodiazepine receptor sites in the human brain: autoradiographic mapping. *Neuroscience* **25**, 771–796.

Zhong P, Gu Z, Wang X, Jiang H, Feng J, Yan Z (2003) Impaired modulation of GABAergic transmission by muscarinic receptors in a mouse transgenic model of Alzheimer's diseaese. *J. Biol. Chem*. **278**, 26888–26896.

Zilles K, Schleicher A (1993) Cyto- and myeloarchitecture of human visual cortex and the periodical $GABA_A$ receptor distribution. In *Functional Organization of the Human Visual Cortex* (eds Gulyas B, Ottoson D, Roland P), pp. 111–122. Oxford: Pergamon Press.

Zilles K, Schlaug G, Matelli M, et al. (1995) Mapping of human and macaque sensorimotor areas by integrating architectonic, transmitter receptor, MRI and PET data. *J. Anat*. **187**, 515–537.

Zilles K, Schleicher A (1995) Correlative imaging of transmitter receptor distributions in human cortex. In *Autoradiography and Correlative Imaging* (eds Stumpf W, Solomon H), pp. 277–307. San Diego: Academic Press.

Zilles K, Schleicher A, Langemann C, et al. (1997) Quantitative analysis of sulci in the human cerebral cortex: Development, regional heterogeneity, gender difference, asymmetry, intersubject variability and cortical architecture. *Human Brain Mapping* **5**, 218–221.

Zilles K, Palomero-Gallagher N (2001) Cyto-, myelo- and receptor architectonics of the human parietal cortex. *Neuroimage* **14**, 8–20.

Zilles K, Palomero-Gallagher N, Grefkes C, et al. (2002a) Architectonics of the human cerebral cortex and transmitter receptor fingerprints. Reconciling functional neuroanatomy and neurochemistry. *Eur. Neuropsychopharmacol*. **12**, 587–599.

Zilles K, Schleicher A, Palomero-Gallagher N, Amunts K (2002b) Quantitative analysis of cyto- and receptorarchitecture of the human brain. In *Brain Mapping. The Methods*, 2nd edn (eds Toga AW, Mazziotta JC), pp. 573–602. New York: Academic Press.

Zilles K (in press) Human brain evolution and comparative cyto- and receptorarchitecture. In *From Monkey Brain to Human Brain* (eds Dehaene S, Duhamel J-R, Rizzolatti G, Hauser M), pp. 000–000. Cambridge, MA: MIT Press.